Available online at www.sciencedirect.com
ScienceDirect
Microporous and Mesoporous Materials xxx (2007) xxx–xxx
MICROPOROUS AND MESOPOROUS MATERIALS
www.elsevier.com/locate/micromeso

Visible-light photocatalytic activity of TiO_2/ZnS nanocomposites prepared by homogeneous hydrolysis

Václav Štengl *, Snejana Bakardjieva, Nataliya Murafa, Vendula Houšková, Kamil Lang

Institute of Inorganic Chemistry AS CR v.v.i., 250 68 Řež, Czech Republic

Received 11 May 2007; received in revised form 5 June 2007; accepted 14 June 2007

Abstract

Photocatalytic active TiO_2/ZnS composites were prepared by homogeneous hydrolysis of mixture of titanium oxo-sulphate and zinc sulphate in aqueous solutions with thioacetamide. The prepared samples were characterized by X-ray diffraction (XRD), scanning electron microscopy (SEM), high resolution transmission microscopy (HRTEM) and electron diffraction (ED). The nitrogen adsorption–desorption was used for surface area (BET) and porosity determination. Diffuse reflectance UV/VIS spectra for evaluation of photophysical properties were recorded in the diffuse reflectance mode (R100) and transformed to an absorption spectra through the Kubelka–Munk function. The method of UV/VIS diffuse reflectance spectroscopy was employed to estimate band-gap energies of the prepared TiO_2/ZnS nanocomposites. The photoactivity of the prepared TiO_2/ZnS nanocomposites was assessed by the photocatalytic decomposition of Orange II dye in an aqueous slurry under irradiation of 255 nm, 365 nm and 400 nm wavelength. Under the same conditions, the photocatalytic activity of the commercially available photocatalyst (Degussa P25), the pure anatase TiO_2 and sphalerite ZnS were also examined. The composite sample having the highest catalytic activity was obtained by hydrolysis of mixture solutions 0.63 M $TiOSO_4$ and 0.08 M $ZnSO_4 \cdot 7H_2O$.

Keywords: Anatase; Sphalerite; Visible-light photocatalytic activity; Homogeneous hydrolysis; Thioacetamide

1. Introduction

TiO_2 and ZnS have been widely used in the field of environmental catalysis [1–3]. However, they are photoactive in the near-UV areas, therefore only 3–4% of solar light is utilized. It is expected that the photocatalytic activity of the solitary TiO_2 will be improved greatly via preparation of the nanoscale coupled semiconductors.

ZnS nanoparticles less of 3 nm average diameter were synthesized by a solvothermal reaction with zinc acetate [$Zn(CH_3COO)_2 \cdot 2H_2O$] and thiourea at 120 °C. Their photophysical properties were investigated. The UV–vis spectrum showed an absorption shoulder at 276 nm, corresponding to the band-gap energy of 4.49 eV, and a weak shoulder at 320 nm (band-gap energy 3.88 eV) [4]. ZnS quantum dots with mercaptoacetic acid as a stabilizer were synthesized by Wageh et al. [5] The solution of $Zn(CH_3COO)_2 \cdot 2H_2O$ and mercaptoacetic acid in dimethylformamide was adjusted to pH 8 by adding 2 M NaOH solution, followed by the dropwise addition of an aqueous solution of sodium sulfide ($Na_2S \cdot 9H_2O$) under vigorous stirring in an N_2 atmosphere. The quantum dots had a diameter of less than 4 nm and a band gap of about 4.2 eV. In a sol–gel process, metal acetates reacted with thioacetamide to form the corresponding metal sulphides homogeneously dispersed in a colloid. The as-prepared dry gels were decomposed by heat treatment at 120 °C to form MS/TiO_2 (M = Pb, Zn, Cd) nanocomposites [6]. Photoactive ZnS/TiO_2 nanocomposites were prepared via microemulsion-mediated solvothermal method. Titanium tetraisopropoxide was added to an inverse emulsion containing water dispersed in a cyclohexane, using Triton

* Corresponding author. Tel.: 420 2 6617 3534; fax: 420 2 2094 0157.
E-mail address: stengl@iic.cas.cz (V. Štengl).

1387-1811/$ - see front matter © 2007 Elsevier Inc. All rights reserved.
doi:10.1016/j.micromeso.2007.06.052

X-100 as surfactant and 1-pentanol as the co-surfactant. This microemulsion was stirred vigorously for 30 min, and $Zn(NO_3)_2$ and $(NH_4)_2S$ were added during stirring [7]. Preparation TiO_2–ZnS composite particles by fluidized chemical vapour deposition technology was described in paper [8]. Nanoporous TiO_2 network sensitized by ZnS nanospheres was prepared from titanium isopropoxide [Ti(i-OC_3H_7)] and 1-butanol as requisite precursor. The Zn^{++} ions are internally adsorbed to provide heterogeneous coupled TiO_2–ZnS nanosystem [9]. The mixed semiconductor (CdS–ZnS)–TiO_2 (1:1:1) mixture system over different supports like MgO, CaO, γ-Al_2O_3, SiO_2 and modified MgO and CaO, have been prepared, characterized and tested for photocatalytic hydrogen production [10].

As it has been shown earlier [11,12] the homogeneous precipitation with urea leads to anatase nanoparticles assembled into a rather big (1–2 μm) porous clusters embodied good photocatalytic properties. Substitution of urea we used the modified homogeneous precipitation with thioacetamide to prepare TiO_2/ZnS nanocomposites. In the same way as the urea method, the homogeneous precipitation of metal sulphides by thermal decomposition of thioacedamide (TAA) can be used [13]. Thioacetamide at temperature higher than 60 °C in acidic solution released sulfan:

$$CH_3CSNH_2 + H_2O \rightarrow CH_3CONH_2 + H_2S \quad (1)$$

$$H_2S + H_2O \rightarrow HS^- + H_3O^+ \quad (2)$$

$$Me^{2+} + HS^- \rightarrow MeS \quad (3)$$

The reaction of products are nanosized spherical particles [14] with a well-developed microstructure, but different from homogeneous urea precipitation. These products have high specific surface area and are properly washed and filtered. In the reaction conditions, the spherical agglomerates of titania are formed by thermal hydrolysis of titanyl sulphate [15] and agglutinated with spherical agglomerates of ZnS, precipitated with thioacetamide. As-prepared TiO_2/ZnS nanocomposites by homogeneous hydrolysis with thioacetamide exhibited new optical properties concerning about the absorption, which were different from those of the bulk anatase[16] or sphalerite [17]. The UV and visible-light photocatalytic activity of the TiO_2/ZnS was tested in the degradation of a 0.02 M Orange II dye aqueous solutions. Under the same conditions, the photocatalytic activity of the commercially available photocatalyst (Degussa P25), the pure anatase TiO_2 and sphalerite ZnS were also examined.

2. Experimental

2.1. Synthesis of TiO_2/ZnS nanocomposites

All used chemicals, titanium oxo-sulphate, zinc sulphate and thioacetamide (TAA) were of analytical grade and were supplied by Fluka. $TiOSO_4$ and $ZnSO_4 \cdot 7H_2O$ (see Table 1) were dissolved in 4 l of distilled water and 100 g thioacetamide was added. The reaction mixture was adjusted to the pH 2 with sulphuric acid. The reaction mixture was heated at 100 °C under stirring for 4 h. Thus synthesized samples were washed by distilled water, filtered off and dried at 105 °C in oven. By this method it was prepared ten samples of TiO_2/ZnS nanocomposites, denoted as TZS_1–TZS_10.

2.2. Characterization methods

Surface area of the samples outgassed for 15 min at 120 °C was determined from nitrogen adsorption-desorption isotherms at liquid nitrogen temperature using a Quantachrom Nova2000 instrument. Langmuir B.E.T. method was used for surface area calculation [18], while pore size distribution (pore diameter and volume) was determined by the B.J.H. method [19].

Transmission electron microscopy (TEM and HRTEM) micrographs were obtained by using two instruments, namely Philips EM 201 at 80 kV and JEOL JEM 3010 at 300 kV (LaB_6 cathode). Copper grid coated with a holey carbon support film was used to prepare samples for the

Table 1
Experimental conditions, crystallite size, surface areas and porosity of prepared samples

Samples	$TiOSO_4$ [g]	$ZnSO_4$ [g]	EDX of Zn [wt.%]	Anatase crystallite size [nm]	Sphalerite crystallite size [nm]	Anatase by XRD [%]	Sphalerite by XRD [%]	BET [$m^2\ g^{-1}$]	Pore radius [nm]	Total pore volume [$cc\ g^{-1}$]
TZS_0	0	100	–	–	16.3	0	100	241.8	0.19	0.061
TZS_1	4	96	78.92	–	15.4	4.4	95.6	89.9	0.18	0.020
TZS_2	9	91	70.25	–	15.9	11.2	88.8	119.8	0.17	0.022
TZS_3	18	82	43.02	7.1	12.7	18.6	81.4	273.8	0.16	0.036
TZS_4	36	64	33.52	3.8	18.4	35.1	64.1	204.3	0.17	0.063
TZS_5	50	50	21.19	6.7	15.2	78.2	21.8	197.1	0.17	0.029
TZS_6	75	25	1.55	5.6	–	100	0	356.2	0.17	0.048
TZS_7	85	15	1.44	6.4	–	100	0	340.2	0.15	0.036
TZS_8	90	10	0.50	6.3	–	100	0	285.8	0.17	0.031
TZS_9	95	5	0.26	6.3	–	100	0	227.9	0.17	0.023
TZS_10	97	3	0.12	6.3	–	100	0	279.4	0.17	0.029
TZS_11	100	0	–	6.5	–	100	0	444.5	0.15	0.082

Please cite this article in press as: V. Štengl et al., Micropor. Mesopor. Mater. (2007), doi:10.1016/j.micromeso.2007.06.052

TEM observation. A powdered sample was dispersed in ethanol and the suspension was treated in an ultrasonic bath for 10 min.

Scanning electron microscopy (SEM) studies were performed using a Philips XL30 CP microscope equipped with EDX (energy dispersive X-ray), Robinson, SE (secondary electron) and BSE (back-scattered electron) detectors. The sample was placed on an adhesive C slice and coated with Au-Pd alloy 10 nm thick layer.

X-ray diffraction (XRD) patterns were obtained by Siemens D5005 instrument using Cu Kα radiation (40 kV, 30 mA) and diffracted beam monochromator. Qualitative analysis was performed with the Eva Application and the Xpert HighScore using the JCPDS PDF-2 database [20]. The crystallite size of the samples was calculated from the Scherrer equation [21] using the X-ray diffraction peak at $2\Theta = 25.4°$ (anatase) and at $2\Theta = 28.6°$ (sphalerite).

Diffuse reflectance UV/VIS spectra for evaluation of photophysical properties were recorded in the diffuse reflectance mode (R) and transformed to absorption spectra through the Kubelka-Munk function [22]. A Perkin Elmer Lambda 35 spectrometer equipped with a Labsphere RSA-PE-20 integration sphere with $BaSO_4$ as a standard was used.

Photocatalytic activity of samples was assessed from the kinetics of the photocatalytic degradation of 0.02 M Orange 2 dye (OII) in aqueous slurries. Kinetics of the photocatalytic degradation of aqueous Orange II dye solution, was measured by using a self-constructed photoreactor [23]. The photoreactor consists of a stainless steel cover and quartz tube with florescent lamp (254 nm, 365 nm and 400 nm) with power 8 W. Orange II dye solution circulated by means of membrane pump through flow cuvette. The concentration of Orange II dye was determined by measuring absorbance at 480 nm with VIS spectrofotometer ColorQuestXE.

3. Results and discussion

3.1. X-ray diffraction (XRD)

The powder XRD patterns of the TiO_2/ZnS composite prepared by homogeneous hydrolysis of sulphates with thioacetamide are shown in Fig. 1. From the XRD patterns and the corresponding characteristic 2Θ values of the diffraction peaks, it can be confirmed that TiO_2 in as prepared samples is identified as anatase-phase (ICDD PDF 21-1272), while the ZnS is sphalerite-phase (ICDD PDF 5-0566). No other polymorph of titania are observed. The broadening of diffraction peaks indicates small size of nanocrystals TiO_2/ZnS composite. The average size t of crystallites was calculated from the peak half-width B, using the Sherrer equation [21],

$$t = \frac{k\lambda}{B\cos\Theta}, \quad (4)$$

where k is a shape factor of the particle (it is *1* if the spherical shape is assumed), λ and Θ are the wavelength and the incident angle of the X-rays, respectively. The peak width was measured at half of the maximum intensity. The crystallite size was calculated from diffraction plane (1 0 1) of anatase (aprox. 6 nm) and diffraction plane (1 1 1) of sphalerite (aprox. 15 nm). The relative amount of anatase and sphalerite was calculated from XRD patterns by PowderCell for Windows version 2.1. programme. (see Table 1.) The relative amount of sphalerite phase in the TiO_2/ZnS nanocomposites decreased from 95.6 to 21.8%.

3.2. Surface area and porosity

BET Langmuir surface area of TiO_2/ZnS composites depend on the amount of TiO_2, the largest surface area ($356.2\ m^2\ g^{-1}$) has sample denoted as TZS_ 6 (see Table 1). TiO_2/ZnS nanocomposites displayed a type I isotherm with desorption hysteresis loop A [24]. Type a hysteresis is due principally to cylindrical pores open at both ends and the microporosity of pore size distribution is under pore diameter 6 nm. Results from desorption BJH pore volume distribution and pore area distribution confirmed microporous structure of prepared samples. Pore radius is 0.17 nm and total pore volume is in interval 0.02–$0.06\ cc\ g^{-1}$ for TiO_2/ZnS nanocompsites.

3.3. Scanning electron microscopy (SEM)

The SEM micrographs of the prepared TiO_2/ZnS nanocomposites are presented in Fig. 2b–k, Zn content is presented in Table 1, as obtained from EDX analysis. The product of homogeneous precipitation of thioacetamide and zinc sulphate consists of approximately spherical round particle agglomerates of diameter about 1–2 μm (Fig. 2a) are formed from laminar nanoparticles of size 16 nm joined to the chains [14]. The products of homogeneous hydrolysis of thioacetamide and titanium oxo-sulphate are 1μm spherical agglomerates formed with 6 nm nanoparticles (Fig. 2l). The TiO_2/ZnS composites are formed as mixture of single TiO_2 or ZnS agglomerates and overgrown TiO_2 and ZnS agglomerates (see Fig. 2b–k).

3.4. Transmission electron microscopy (TEM and HRTEM)

Results obtained by high resolution transmission electron microscopy (HRTEM) and electron diffraction (ED) are shown in Figs. 3–5. The HRTEM micrographs in Fig. 3a–d correspond to the surface morphology of the sample denoted TZS_6. The sample TZS_6 is consist of alternate nanosized titania and sphalerite crystalline islands. The interlayer spacing $d = 0.35$ nm, corresponding to the (1 0 1) plane of anatase (Fig. 3c), while the interlayer spaces 0.19 nm and 0.31 nm, respectively, corresponding to the (2 2 0) and (1 1 1) planes of sphalerite (Fig. 3d).

Diffraction methods are the most important sources of structure information to identify individual microscopic-

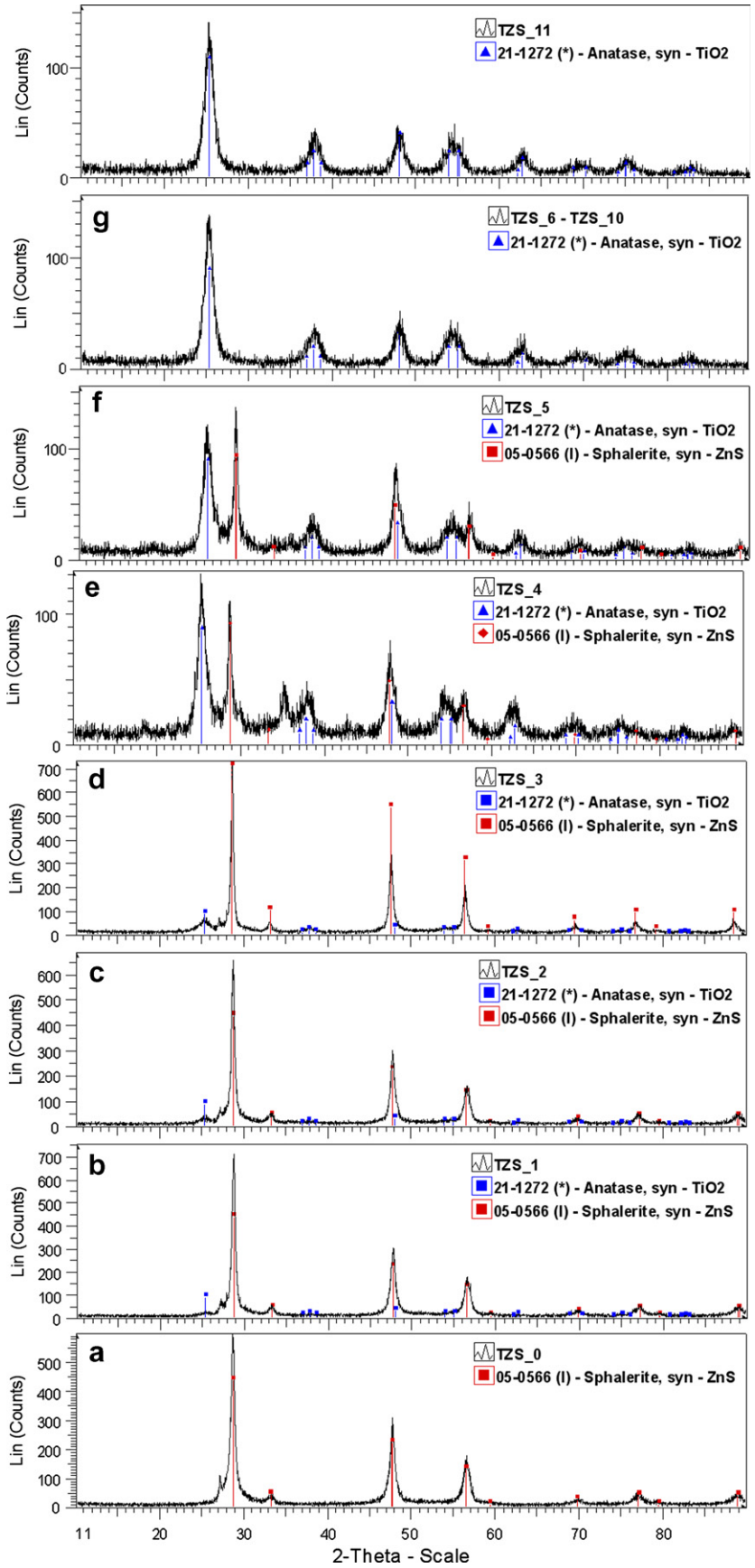

Fig. 1. XRD pattern of (a) sample ZnS denoted as TZS_0, (b–k) sample TiO_2/ZnS denoted as TZS_1–TZS_10, (l) sample TiO_2 denoted as TZS_11.

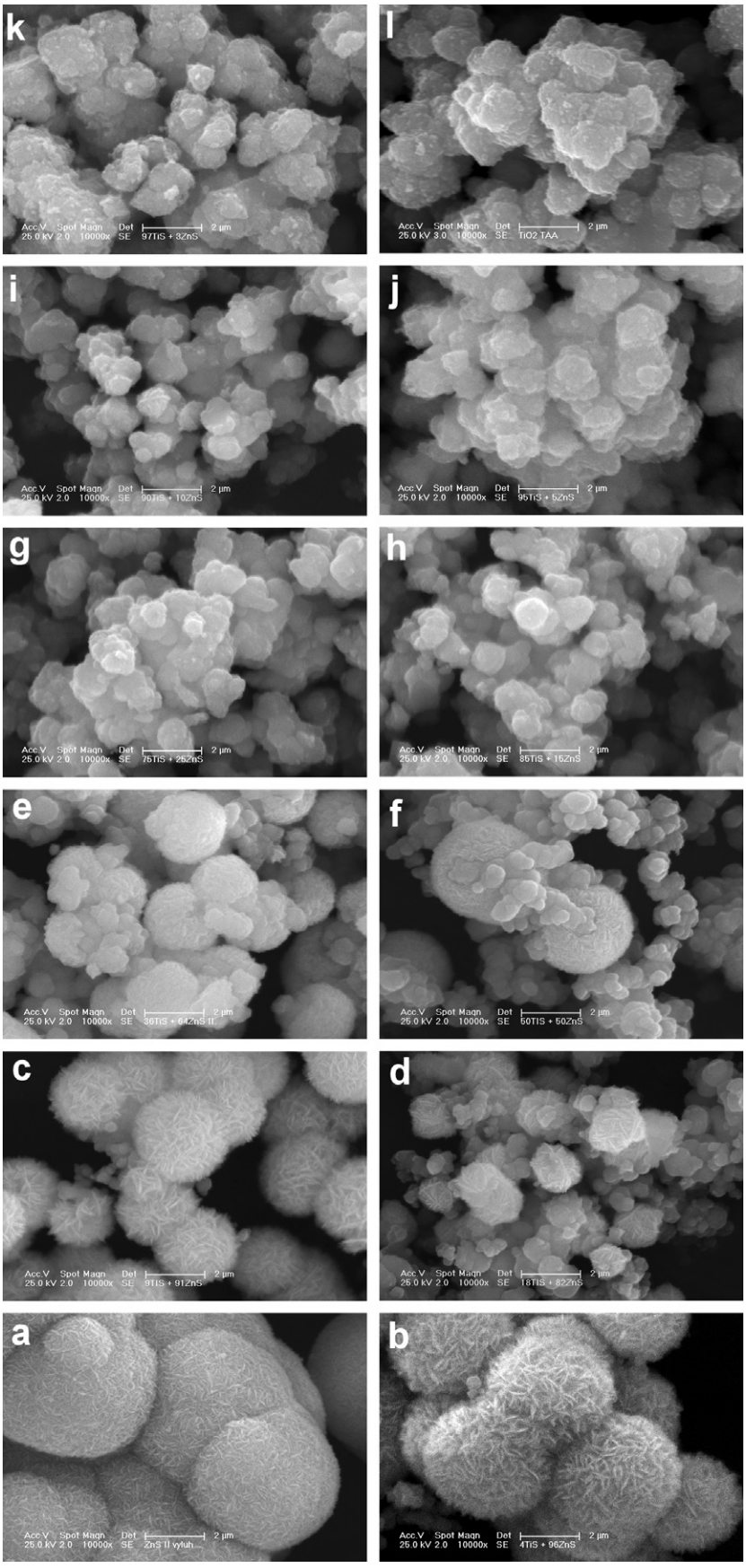

Fig. 2. SEM images of (a) sample ZnS denoted as TZS_0, (b–k) sample TiO_2/ZnS denoted as TZS_1–TZS_10, (l) sample TiO_2 denoted as TZS_11.

Please cite this article in press as: V. Štengl et al., Micropor. Mesopor. Mater. (2007), doi:10.1016/j.micromeso.2007.06.052

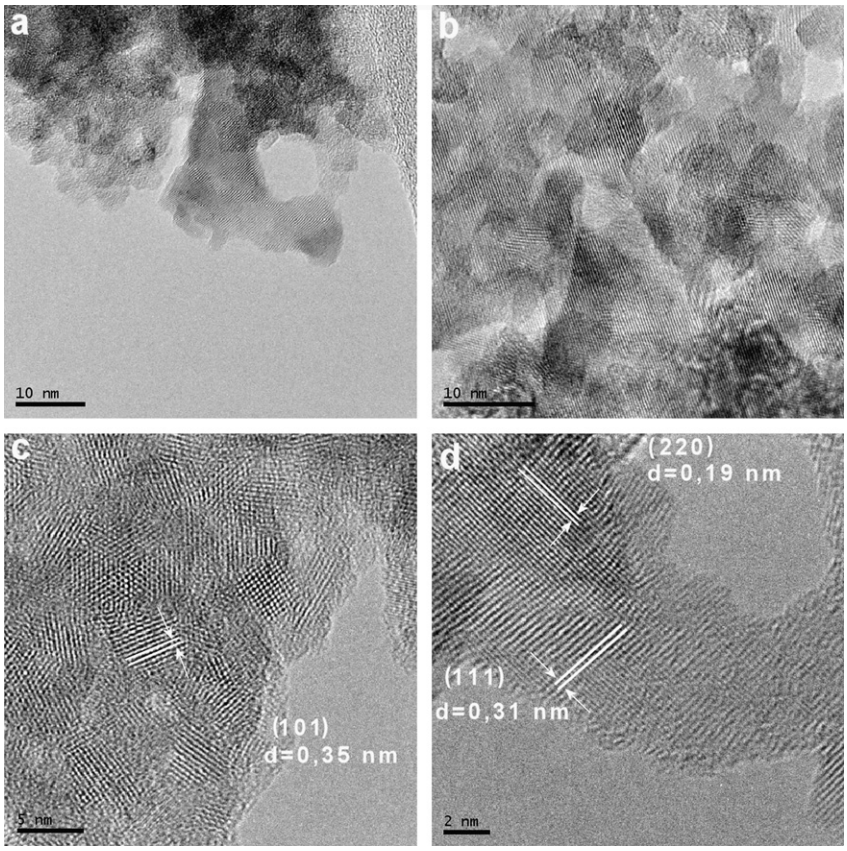

Fig. 3. HRTEM micrographs of TiO_2/ZnS nanocomposite sample denoted as TZS_6, magnification 300,000 (a) Images (b), (c) and (d) are enlarged parts of the image (a).

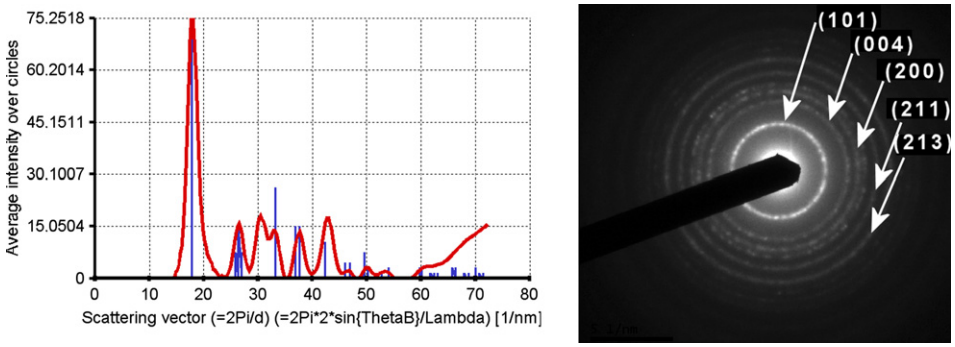

Fig. 4. Electron diffraction pattern of sample denoted as TZS_6 (anatase). The ED pattern was treated using software process diffraction.

sized crystallites, i.e. to identify the crystallographic phase the crystallite corresponds to. Structure determination is generally based on selected area electron diffraction (SAED) patterns in the transmission electron microscope (TEM). A computer program called Process Diffraction [25] helps indexing a set of single crystal selected area electron diffraction (SAED) patterns by determining which of the presumed structures can fit all the measured patterns simultaneously. Distances and angles are measured in the digitalized patterns with a graphical tool by clicking on the two shortest non-collinear vectors (spots), using user-supplied calibration data. Next figures depicts the selected electron diffraction patterns (SAED) analyzed by Process Diffraction program and Fig. 4 resulted that the structure of the sample is anatase (ICDD PDF 21-1272) and Fig. 5 showing that the structure is sphalerite (ICDD PDF 05-0566).

3.5. UV/VIS spectra and band-gap energy

Fig. 6 presents UV/VIS absorption spectra of the prepared samples. The prepared TiO_2/ZnS nanocomposites

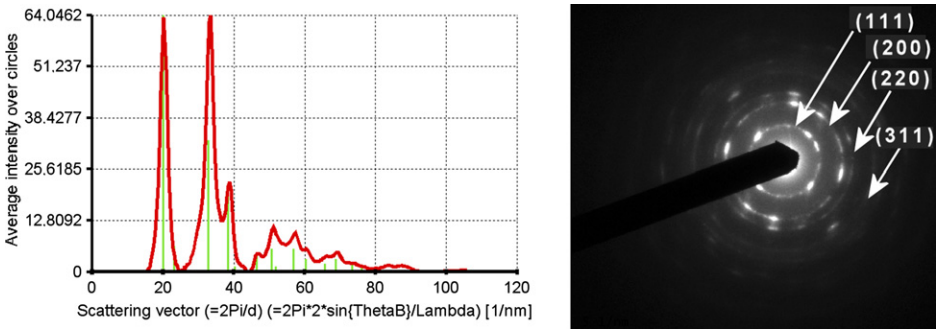

Fig. 5. Electron diffraction pattern of sample denoted as TZS_6 (sphalerite). The ED pattern was treated using software process diffraction.

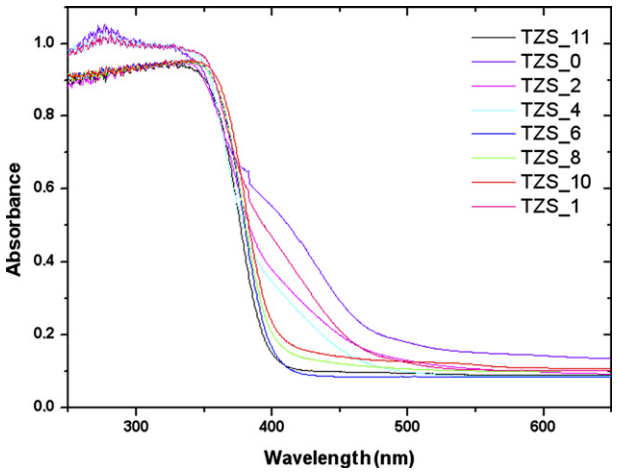

Fig. 6. Absorbance UV/VIS spectra as prepared TiO_2/ZnS nanocomposites.

exhibit new optical properties concerning about the absorption, which are different from those of the TiO_2 or ZnS. The anatase has a wide absorption band in the range from 200 to 385 nm and the ZnS has a UV absorption band in the range from 200 to 338 nm [26]. Fig. 6 shows that the diffuse reflectance spectra of the prepared TiO_2/ZnS nanocomposites and pure ZnS, respectively, denoted as TZS_0 is red-shifted in the sequence of TZS_11 → TZS_0, where the amount of anatase decreased. These may be generated by sulphur compounds such as polysulphides as already observed for zinc sulphide [27] and it is due to the agglomeration of nanoparticles. It is note worthy that sample denoted TZS_0 is slightly yellow coloured.

Compared with the TiO_2 and ZnS, the red-shift of the UV absorption band happened for the TiO_2/ZnS nanocomposites. The red-shift be joined by growth particles [28], the blue-shift is caused by the strong quantum confinement effect, suggesting that the sizes of particles are in the nanoscale [29].

The method of UV/VIS diffuse reflectance spectroscopy was employed to estimate band-gap energies of the prepared TiO_2/ZnS nanocomposites. Firstly, to establish the type of band-to-band transition in these synthesized particles, the absorption data were fitted to equations for direct band-gap transitions. The minimum wavelength required to promote an electron depends upon the band-gap energy E_{bg} of the photocatalyst and is given by:

$$E_{bg} = 1240/\lambda[\text{eV}], \quad (5)$$

where λ is the wavelength in nanometers [2,30].

Fig. 7 shows the $(\alpha E_{bg})^2$ versus E_{bg} for a indirect band-gap transition, where α is the absorption coefficient and E_{bg} is the photon energy. The value of E_{bg} extrapolated to $\alpha = 0$ gives an absorption energy, which corresponds to a band-gap energy (see Table 2). The value of 3.20 eV for sample denoted as TZS_11 is reported in the literature for pure TiO_2 anatase nanoparticles [2], the value of band-gap energy decreases with increasing content of ZnS. The density of the yellow colour of prepared samples depends on the content of ZnS. The sulphur from ZnS is able to doping of the surfaces titania particles [31,32] and decreases the value of band-gap energy.

3.6. Photocatalytic activity

The photocatalytic activity of the prepared samples was determined by the degradation of 0.02 M Orange II dye aqueous solutions under UV radiation (at 254 nm and 365 nm) and VIS radiation (over 400 nm). In regions where

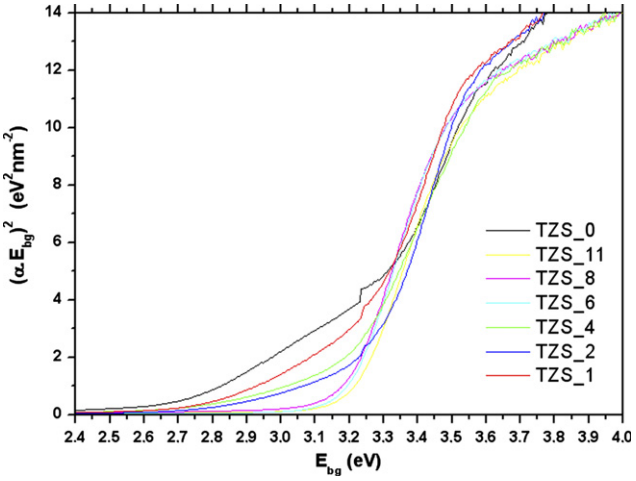

Fig. 7. Band-gap energy as prepared TiO_2/ZnS nanocomposites.

Table 2
The band-gap E_{bg} and rate constant k at 255 nm, 365 nm and 400 nm wavelength

Sample	Bandgap [eV]	Rate constant at 255 nm [min^{-1}]	Rate constant at 365 nm [min^{-1}]	Rate constant at 400 nm [min^{-1}]
TZS_0	2.4	0.0578	0.0091	0.0033
TZS_1	2.5	0.0401	0.0089	0.0036
TZS_2	2.5	0.0384	0.0199	0.0245
TZS_3	2.6	0.0366	0.0222	0.0070
TZS_4	2.7	0.0376	0.0068	0.0022
TZS_5	2.8	0.0477	0.0268	0.0248
TZS_6	2.9	0.1082	0.0332	0.0381
TZS_7	2.9	0.0514	0.0117	0.0069
TZS_8	2.9	0.0478	0.0142	0.0100
TZS_9	2.9	0.0763	0.0248	0.0087
TZS_10	2.9	0.1689	0.0253	0.0027
TZS_11	3.2	0.0817	0.0340	0.0009
P25 Degussa	3.1	0.0647	0.0471	0.0022

the Lamber-Beer law is valid, the concentration of the Orange II dye is proportional to absorbance.

$$A = \epsilon\ c\ l, \tag{6}$$

where A is absorbance, c is concentration of absorbing component, l is length of absorbing layer and ε is molar absorbing coefficient. The time dependences of Orange II dye decomposition can be described by using Eq. (7) for the first kinetics reaction [33]:

$$\frac{d[OII]}{dt} = k(a_0 - [OII]), \tag{7}$$

where [OII] is concentration of Orange II dye, a_0 is initial concentration of Orange II dye and k is rate constant. It is visible from Fig. 8, that the first order kinetics curves (plotted as lines) fitted to all experimental points. For comparison, the photocatalytic activity of a commercially available photocatalyst (Degussa P25), anatase TiO_2 or ZnS nanoparticles was also tested. The calculated degradation rate constants are listed in Table 2 and example of kinetic degradation the sample denoted TZS_6 and P25 of Orange II dye at 254 nm, 365 nm and 400 nm wavelength is presented in Fig. 8.

From Table 2 is followed, that pure anatase (sample denoted TZS_11) and Degussa P25, respectively, exhibits very low visible-light photocatalytic activity for aqueous Orange II dye degradation because the band-gap energy of Degussa P25 is of 3.1 eV ($\lambda_{bg} = 400$ nm) [34] that possibly reflects its phase composition (80% anatase and 20% rutile), corresponding to absorption in the near UV region. The band-gap energy of bulk ZnS is 3.7 eV ($\lambda_{bg} = 335$ nm), for anatase it is 3.2 eV ($\lambda_{bg} = 388$ nm) and rutile = 3.0 eV ($\lambda_{bg} = 413$ nm) [2]. As for the nanoscale ZnS (sample denoted TZS_0), it exhibits some activity for degradation of the Orange II dye although its band-gap energy is relatively high. The sample denoted TZS_6 shows the highest photoactivity, this results probably corresponds with the high surfaces area (356 $m^2\ g^{-1}$). UV light provides the photons required for the electron transfer from valence band to conduction band of the photocatalyst. The energy of a photon is related to its wavelength and the overall energy input to a photocatalytic process is dependent upon the light intensity. Therefore, the effect of both intensity and wavelength are important. Matthews and McEvoy [35] showed that shorter wavelength (254 nm) radiation is considerably more effective in promoting degradation than

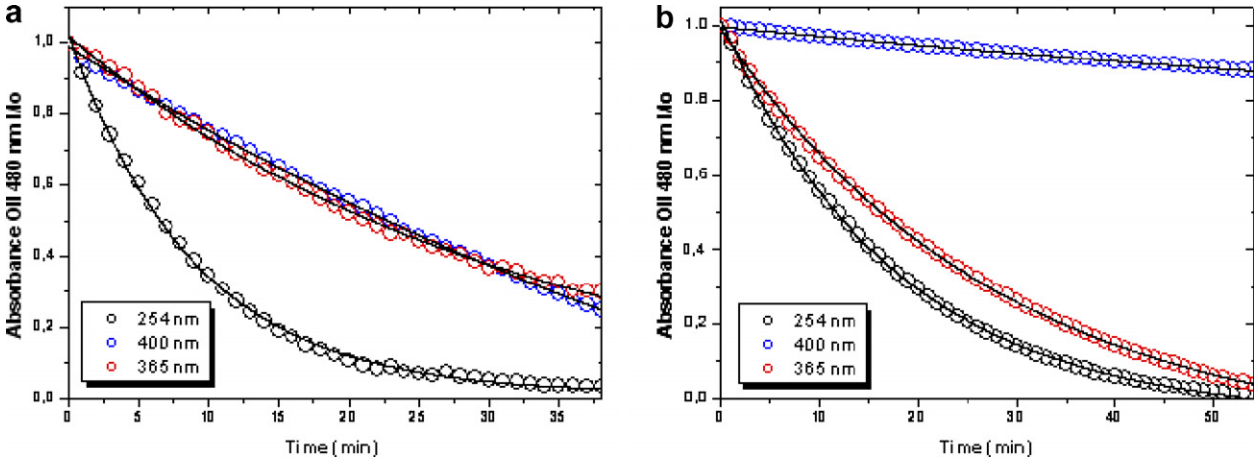

Fig. 8. Photocatalytic activity at wavelengths 254 nm, 365 nm and 400 nm (a) sample denoted TZS_6, (b) P25 Degussa.

radiation centred at 350 nm and the optimum rate occurred with a lower catalyst loading than required at 350 nm. Hofstadler et al. [36] also showed that shorter wave lengths resulted in higher photocatalytic degradation process rates of 4-chlorophenol with small amounts of intermediates being formed. This is due to the fact that shorter wavelength is associated with greater photon energy. All prepared TiO_2/ZnS nanocomposites embodied high photocatalytic activity at 400 nm of wavelength, enhancement photocatalytic activity in visible light area demonstrate decrement photocatalytic activity in UV area. These results are conformable with the red-shift in absorbance spectra and with decrement of band-gap energy (see Figs. 6 and 7).

4. Conclusion

This paper presents a simple method for preparation of the efficient photocatalytic materials, TiO_2/ZnS nanocomposites by method of homogeneous hydrolysis in aqueous solutions with thioacetamide. The prepared composites exhibit better UV characteristic compared with the bulk TiO_2 and ZnS. The nanocomposites show efficient visible-light photocatalytic activity to degrade the aqueous solution of Orange II dye, which is higher than that of a commercially available TiO_2 (Degussa P25), pure anatase TiO_2, or cubic ZnS nanoparticles. The composite sample having the highest catalytic activity was obtained by hydrolysis of mixture solutions 0.63 M $TiOSO_4$ and 0.08 M $ZnSO_4 \cdot 7H_2O$.

Acknowledgment

This work was supported by the Academy of Sciences of the Czech Republic (Project No. AV OZ 40320502).

References

[1] A. Fujishima, T.N. Rao, D.A. Tryk, Journal of Photochemistry and Photobiology C: Photochemistry Reviews 1 (2000) 1–21.
[2] D.S. Bhatkhande, V.G. Pangarkar, A.A. Beenackers, Journal of Chemical Technology and Biotechnology 77 (2001) 102–116.
[3] M. Vautier, C. Guillard, J.M. Herrmann, Journal of Catalysis 201 (2001) 46–59.
[4] Y. Li, Y. Ding, Y. Zhang, Y. Qian, Journal of Physics and Chemistry of Solids 60 (1999) 13–15.
[5] S. Wageh, Z.S. Ling, X.X. Xu Xu-Rong, Journal of Crystal Growth 255 (2003) 332–337.
[6] H. Su, Y. Xie, P. Gao, Y. Xiong, Y. Qian, Journal of Material Chemistry 11 (2001) 84.
[7] Y. Xiaodan, W. Qingyin, J. Shicheng, G. Yihang, Materials Characterization 57 (2006) 333–341.
[8] Z. Hai-sheng, W. Rui, J. Rui-bao, Materials Science and Technology 3 (2005) 261–263.
[9] D. Mohanta, M. Deka, A. Choudhury, Journal of Applied Physics 101 (2007) 044302–044304.
[10] S.V. Tambwekar, D. Venugopal, M. Subrahmanyam, International Journal of Hydrogen Energy 24 (1999) 957–963.
[11] V. Stengl, J. Subrt, P. Bezdicka, S. Bakardjieva, J. Subrt, Solid State Phenomena 90–91 (2003) 121–126.
[12] S. Bakardjieva, V. Stengl, J. Subrt, Solid State Sciences 7 (2005) 367–374.
[13] T. Nomura, Y. Kousaka, M. Alonso, M. Fukunaga, Journal of Colloid and Interface Science 223 (2000) 179–184.
[14] V. Housková, V. Štengl, S. Bakardjieva, N. Murafa, A. Kalendová, F. Opluštil, Journal of Physical Chemistry A 111 (2007) 4215.
[15] V.A. Yasir, P.N. MohanDas, K.K.M. Yusuff, International Journal of Inorganic materials 3 (2001) 593–596.
[16] S. Bakardjieva, V. Štengl, J. Šubrt, M.J. Diane, M.J. Sayagues, Applied Catalysis B: Environmental 58 (Issues) (2005) 193–202.
[17] V. Housková, V. Štengl, S. Bakardjieva, N. Murafa, K. Kalendová, F. Opluštil, Journal of Physics and Chemistry of Solids 68 (2007) 707.
[18] S. Brunauer, P.H. Emmett, E. Teller, Journal of the American Chemical Society 60 (1938) 309.
[19] E.P. Barret, L.G. Joyner, P.P. Halenda, Journal of the American Chemical Society 73 (1951) 373.
[20] JCPDS PDF-2 release 2001, ICDD Newtown Square, PA, USA.
[21] P. Scherrer, Gottinger Nachrichte 2 (1918) 98.
[22] Z.C. Orel, M.K. Gunde, B. Orel, Progress in Organic Coatings 30 (1997) 59–66.
[23] V. Štengl, S. Bakardjieva, N. Murafa, V. Balek, V. Havlín, Optically transparent titanium dioxide particles incorporated in hydroxyethyl methacrylate thin layers, in press.
[24] S. Lowell, J.E. Shields, Powder Surface Area and Porosity, Chapman & Hall, 1998.
[25] J.L. Labár, Ultramicroscopy 103 (2005) 237.
[26] H. Yin, Y. Wada, T. Kitamura, S. Yanagida, Environmental Science & Technology 35 (2001) 227–231.
[27] R. Kiinnetha, G. Twardzik, G. Emigb, H. Kischa, Journal of Photochemistry and Photobiology A: Chemistry 76 (1993) 209–215.
[28] L. Wan, J.F. Li, J.Y. Feng, W. Sun, Z.Q. Mao, Applied Surface Science 253 (2007) 4764–4767.
[29] K.M. Reddy, C.V. Gopal Reddy, S.V. Panorama, Journal of Solid State Chemistry 158 (2001) 180–186.
[30] K.M. Reddy, S.V. Panorama, A.R. Reddy, Materials Chemistry and Physics 78 (2002) 239–245.
[31] T. Ohno, M. Akiyoshi, T. Umebayashi, K. Asai, T. Mitsumi, M. Matsumura, Applied Catalysis A: General 26 (2004) 115–121.
[32] W. Ho, J.C. Yu, S. Lee, Journal of Solid State Chemistry 179 (2006) 1171–1176.
[33] M. Macounová, H. Krýsová, J. Ludvík, J. Jirkovský, Journal of Photochemistry and Photobiology A: Chemistry 156 (2003) 273.
[34] K. Nagaveni, G. Sivalingan, M.S. Hegde, G. Madras, Applied Catalysis B: Environmental 48 (2004) 83.
[35] R.W. Matthews, S.R. McEvoy, Journal of Photochemistry and Photobiology A: Chemistry 66 (1992) 355–366.
[36] K. Hofstadler, R. Bauer, S. Novalic, G. Heisler, Environmental Science & Technology 28 (1994) 670–674.